

Lawrence Livermore Laboratory

EVALUATION OF MATERIALS EXPOSED TO HIGH-VELOCITY,
HIGH-SALINITY, HIGHLY MINERALIZED GEOTHERMAL BRINE

Alfred Goldberg and Robert P. Kershaw

August 20, 1978

This paper was prepared for the Eleventh International
Metals Society Technical Meeting, Montreal, Canada,
July 16-19, 1978

This is a preprint of a paper intended for publication in a journal or proceedings. Since changes may be made before publication, this preprint is made available with the understanding that it will not be cited or reproduced without the permission of the author.



EVALUATION OF MATERIALS EXPOSED TO HIGH-VELOCITY, HIGH-SALINITY,
HIGHLY MINERALIZED GEOTHERMAL BRINE*

Alfred Goldberg and Robert P. Kershaw

Lawrence Livermore Laboratory, University of California
Livermore, California 94550

ABSTRACT

Using surface traces, scanning electron microscopy, and light microscopy, Ti-, Co-, Ni-, and Fe-base alloys were evaluated for erosion and stress corrosion cracking (SCC) after exposure at about 104°C to the nozzle exhaust from acidified geothermal brine. Examples of erosion, SCC, and corrosion are shown. Results are evaluated in terms of synergism between erosion, corrosion, and stress. Repassivation kinetics might play a key role in the formation and growth of erosion cavities. Of the materials tested, the Ti-base alloys appear to have the best combination of resistance to SCC and erosion/corrosion in high-salinity, highly mineralized, acidified, two-phase nozzle exhaust.

* Work performed under the auspices of the U.S. Department of Energy by the Lawrence Livermore Laboratory under contract number W-7405-Eng-48.

INTRODUCTION

As part of an experimental program on the use of geothermal brines for electric power production, we performed a number of chemistry and materials tests at the Lawrence Livermore Laboratory (LLL) Field Test Station, which is located near Niland in the Salton Sea Geothermal Field of Southern California. The brines at the test site have a high salinity, are highly mineralized, and are at temperatures approaching 300°C. In one of the energy-conversion systems that was being considered for these brines, the total flow of the wellhead is expanded through converging-diverging nozzles to drive an impulse turbine. During expansion, the cooling and mineral enrichment of the residual liquid results in the deposition of silica-rich scale, which could seriously limit the operation of the turbine system. Acidification of the brines with HCl was investigated as a possible method for reducing and controlling scale deposition. From these scale-control tests, we also derived information on the erosion/corrosion of various alloys exposed to the brine.

This paper describes our analysis of materials exposed to flowing, acidified brine in three series of field tests, where the brine was expanded through converging-diverging nozzles to produce high-velocity, two-phase flow. Most of the materials tested were potential candidates for the total-flow turbine. Details on the complete LLL Geothermal Energy Program, including acidification for scale control and the analysis of scale deposition, are described elsewhere. (1)

EXPERIMENTAL

The quality of the brine at the wellhead was 10 to 20% vapor. To give some control of variables in the system, the liquid phase was separated from the vapor and used as the unmodified starting brine. Acid was introduced 3 m upstream from the nozzles through metering pumps. Three parallel test stations were used simultaneously but controlled independently. In the first test series, acidified 100% liquid (0%-quality brine) was expanded. In the second and third test series, vapor was reintroduced into the acidified brine just ahead of each nozzle. The nozzle-inlet quality for the second test series is estimated at 5%; for the third test series, we calculated qualities of 11% for two stations and 33% for the other station. The brine entered the nozzles under pressures between 1.5 and 2.5 MPa, at about 210°C, and with velocities from about 3 m/s for 0%-quality to about 80 m/s for 33%-quality inlet. In all cases the brine was expanded to atmospheric pressure at about 104°C.

The composition of the brine could vary significantly, not only during a day's testing but also as a result of changes in operating conditions.⁽¹⁾ Table I shows the analyses of brines taken from the LLL separator on four different days. Chlorine and total solids contents ranged from 10 to 15% and 17 to 25%, respectively. The brine is relatively reducing, and the pH is typically close to 5.8.

Figure 1 shows a test assembly used for expanding the brine and for evaluating both scale control and turbine materials. The test assembly is inserted into a 102-mm-diameter pipe elbow, which receives the expanded brine exhaust and also simulates the wall curvature of a turbine chamber. The nozzle, which has an expansion ratio of 8:1, can either be monolithic or have a removable insert. The wearblade, which represents the leading edge of a turbine blade, is 66 mm wide by 44 mm deep. It has a wedge-shaped leading edge, which we specified should have an included angle of 0.35 rad and a tip radius of 254 μm . The tip is located 12.7 mm from the nozzle exit. The velocity of the two-phase nozzle exhaust at the tip was estimated to be 250 m/s for 0%-quality inlet and up to 380 m/s for the two-phase inlet.⁽²⁾

Evaluation of nozzles and wearblades provided information on erosion as well as on scale deposition.⁽¹⁾ We also obtained information on stress corrosion cracking (SCC) from bent-beam, sheet specimens loaded above their yield stress in fixtures attached to the wearblade holder. The SCC specimens were mounted in pairs, one pair on each side of the wearblade, so that the tensile-stressed surface of the front sample was exposed to the direct nozzle exhaust while the corresponding surface of the rear sample was shielded from such impact. The SCC specimens were 76 mm long by 6.4 mm wide, with thicknesses between 0.65 and 2.5 mm; most were about 1.6 mm thick. With few exceptions, specimens contained a machined notch 125 μm deep. The SCC specimens yielded information on erosion and erosion/corrosion as well as on SCC.

Figure 2(a) shows a test assembly following a 20-h exposure to expanded brine. Typical appearances of exposed wearblades are shown in Fig. 2(b) for a steel that was attacked severely by erosion/corrosion and in Fig. 2(c) for a Ti-base alloy that exhibited relatively minor degradation. As seen on the wearblade in Fig. 2(c), the central region that was exposed to the direct nozzle exhaust is clearly outlined by the peripheral scale deposits. Such scale deposits are probably due to splashback from the pipe chamber walls. A relatively thin film of scale can also be seen in the central region.

MATERIALS

Preliminary tests with unmodified brine indicated that Ti-base alloys were the alloys most likely to withstand erosion/corrosion from the high-velocity, nozzle-exhaust fluids. Furthermore, Ti-base alloys exhibit better resistance to SCC in chloride-bearing, aqueous environments than do the Fe-, Ni-, and Co-base alloys. (3-5) Therefore, our tests emphasized the use of Ti-base alloys, especially Ti-6Al-4V and Ti-6Al-4V extra low interstitial (ELI).

Except for two tests using nozzles of Haynes Stellite 6B and Zr-grade CP-702, Ti-6Al-4V was used for all the nozzles. By contrast, many alloys were tested as wearblades and SCC specimens. The specific alloys are given later in the paper.

We had difficulty characterizing our observations in terms of test conditions because these tests were primarily to study scale control. Therefore we could not provide a matrix of controlled variables that would allow for a systematic materials analysis.

Brine conditions frequently varied from test to test and between test stations. The chemistry of even the untreated brine probably varied significantly in such important corroding constituents as S, As, NH_3 , CO_2 , etc. and also probably varied in redox potential, quality, and pH. Finally, exposure periods were not constant. Most of the specimens were exposed for 20 h, several for as little as 7.5 h, and one set for 120 h. Because of these variations, we will emphasize the types of material degradation rather than their ranking, although some ranking will be self-evident.

EVALUATIONS OF EXPOSED MATERIALS

Methods

All specimens were examined using light microscopy. The etchants for specimens shown in the micrographs in this paper were as follows:

Ti-base alloys - Keller's reagent

Inconel 718 - 10 ml HCl + 90 ml methanol, 1 to 2 s at 50 V

Stellite 6B and Haynes 25 - 97 ml HCl + 3 ml of 5% H_2O_2

Hastelloy C-276 - 5% chromic acid, 2 to 10 s at 3 V

MP35N - 50% Fry's reagent + 50% HCl, fresh solution,

vigorously swabbed

304 and 316 stainless steel - Kalling's reagent

Ferritic stainless steels - 10 ml HCl + 90 ml methanol, 3 to

5 s at 6 V

410 stainless steel - 10% FeCl_3 in H_2O

Low-alloy steels - 2% nital

The wearblades were also examined using surface-analysis traces and scanning electron microscopy (SEM); details are given later in this paper. For light microscopy, nozzles and wearblades were sectioned through the center, parallel to the flow axis. Complete nozzle sections were examined, while for wearblades only the exposed tip and an adjacent portion of the leading edge were examined. For SCC specimens, approximately 25 mm of the central part of each specimen was mounted so that the longitudinal-thickness surface could be viewed. Unless otherwise indicated, in all the photomicrographs we present here the brine flow is from top to bottom of the photo for cross-section views and is perpendicular to the photo for SEM views.

Nozzles

Figure 3 shows sections of the Stellite 6B nozzle (R_C 38) exposed to 11%-quality inlet for 60.5 h. The nozzle was eroded just downstream from the throat. Visual observations clearly showed erosion gouges running parallel to the flow direction; these can be seen at a low magnification in view (b) of Fig. 3. View (c) shows the erosion cavities at higher magnification. Some damage is also seen at the nozzle inlet in view (b). The remainder of the nozzle was degraded much less, as shown by the throat region, view (a), and near the nozzle exit, view (d).

Figure 4 shows sections of a Ti-6Al-4V nozzle (R_C 39) exposed to the same nominal conditions and for the same period as the Stellite 6B nozzle. Erosion was absent throughout the nozzle, view (b). An example of the erosion-free surface is shown in view (a),

the nozzle throat. An interesting observation was the formation of an elliptical ridge of scale several millimetres from the exit end, views (b) and (c). This scale was attributed to a shock effect when the pressure of the expanding fluids at this location dropped to the atmospheric chamber pressure.⁽²⁾ Turbulence and an increase in local residence time could cause such scale deposition. A similar ridge was seen in the Zr nozzle (R_C 8) exposed simultaneously in another station. This nozzle also did not suffer any erosion. Such a ridge was probably also present in the Stellite 6B nozzle where the scale had flaked off (Fig. 3(b)). The presence of a ridge suggests that the expected velocities of over 380 m/s were not achieved.⁽²⁾

Wearblades

We had several problems in measuring relative erosion of the leading-edge tips, where most of the erosion takes place. First, the degree of surface roughness and the location and presence of erosion cavities were found to vary with metallographic repolishing. Second, examinations of sections of several unexposed wearblades indicated that the tips were not always machined accurately to the specified 254- μ m radius, resulting in either a flattened or unsymmetrical tip. Although this did not create any problem in the scale-control evaluation part of the program, it did not permit simple evaluation of wearblade erosion by examining surface recession alone. Our evaluations were finally based on a combination of observations using surface traces, SEM, and light microscopy of cross sections.

Surface traces were taken along the tip of the leading edge of wearblades using a Gould Surfalyzer 1200^{*} with a 50-mg diamond tip stylus having a 2.5- μ m tip radius. Scale, if present, was removed from the leading-edge tip using a plastic scraper. The wearblades were then cleaned ultrasonically in a soap solution. Comparisons of traces obtained from specimens before exposure, after exposure, and after removal of scale along the tip surface showed that erosion occurred only in the central region that was exposed to the direct exhaust, and this was confirmed by microscopic examination. Thus, we could measure the extent of erosion by comparing the center of the trace with the extremities of the trace.

In Fig. 5 are portions of traces taken along the tip of Ti-6Al-4V (R_C 36) and Hastelloy C-276 (R_C 46) wearblades exposed for 60.5 and 49.5 h, respectively, both to 11 $\frac{1}{2}$ -quality inlet brine with exhaust pH 2.3.[†] Figures 6 and 7 show cross sections of these two wearblades, confirming the trace results. The

* Reference to a company or product name does not imply approval or recommendation of the product by the University of California or the U.S. Department of Energy to the exclusion of others that may be suitable.

† The pH values are the average of measurements of cooled samples taken from the liquid fraction of the nozzle exhaust.

Ti-6Al-4V alloy eroded very little, with the tip surface receding about 20 μm , while the C-276 alloy eroded by an order of magnitude greater: about 200 μm . In both cases erosion was considerably less along the tapered surfaces than at the tips. Note that the erosion in the C-276 alloy progressed more in the light etching bands than in the dark etching bands (chemical segregation).

Figure 8 shows light microscopy and SEM views of the leading-edge tips for two Ti-6Al-4V-ELI wearblades both exposed to 5% quality inlet with the exhaust pH 3.4, one for 20.1 h (R_C 32), the other for 120.6 h (R_C 34). Both series of SEM photomicrographs show the presence of distinct microscopic cavities present along the entire eroded tip surfaces. Comparing the cross sections and SEM views for the 20.1- and 120.6-h exposures suggests that erosion progresses by the formation and growth of individual microscopic cavities, with recession and flattening of the surface along the center of the tip. The flat regions are the regions between the arrows in views (c) and (d). (The SEM views are at 90° to the cross-section views, and therefore the cavities shown in view (b) correspond to a cross section of the cavities in view (d).) We suggest that the cavities merge and form new surfaces, which are subsequently eroded by formation of new cavities. We estimate the surface recession at 3 and 70 μm and the largest pit depths at 2 and 60 μm for the two wearblades, respectively. The proportions of the damages caused by the long- and short-time exposures are significantly greater than the proportion of the exposure times,

suggesting either a long incubation period (<20 h) or, following an initial roughening of the surface, an acceleration of the rate of erosion during the interval between 20 and 120 h.

In views (g) and (h), the walls of the cavities appear to contain fine, submicron-size cavities, about $1\ \mu\text{m}$ or less in diameter; the small cavities are irregular and somewhat angular, probably reflecting the shape of the impinging particles. In other cases (described later) the fine structure of the wall surfaces has a definite granular appearance but of the same approximate dimensions.

We thought that perhaps the erosion patterns could be related to the microstructure; i.e., that the cavities in view (c) could be related to the coarse primary α grains and those in view (g) to the fine, aged α' martensite. To examine this possibility, we compared the microstructures of an annealed (R_C 10) and of a cold-worked-and-aged (R_C 43) Hastelloy C-276 wearblade exposed for 37 and 20.1 h to 0- and 5%-quality inlets, respectively. We saw little difference in the extent of erosion damage and no difference in the morphology of the cavity walls. Figure 9 shows that the erosion cavities form into erosion channels in these two exposed wearblades. The formation of such channels is probably associated with segregation of the alloy as indicated by the banding seen in views (a) and (b). The annealed wearblade was exposed almost twice as long as the hardened wearblade, although probably to less severe conditions (0 vs 5% quality). We do not think that erosion would

give almost equal damage to the two wearblades in spite of the longer exposure time. Thus corrosion must also play an important role, subduing the expected effect of relative hardness.

The fine structure of the cavity walls, views (e) and (f), appears to consist of angular-shaped grains. We suggest that these grains are "hills" between submicron cavities similar to those seen in the Ti-base alloys. Such angular-shaped grains were observed in all the Ni- and Co-base alloys. Differences between the cavity-wall morphologies of these alloys and the Ti-base alloys might result from differences in the contribution of corrosion to erosion for the two groups of alloys. Initially, we were concerned that the granular structure might be associated with scale. However, energy-dispersive x-ray analysis of a number of specimens verified that this was not the case; a few particles, of the order of 5 to 10 μm , were occasionally identified as scale.

As we indicated previously, erosion was concentrated at the tip of the leading edge; usually there was considerably less erosion along the tapered faces. An extreme exception to this, where the faces have been extensively attacked, is shown in Fig. 10 for quenched-and-tempered 2.2Cr-1Mo steel (R_c 21) exposed 37 h to 0%-quality inlet with exhaust pH 2.6. The exposed wearblade, Fig. 2(c), was covered with a heavy layer of corrosion product and scale. Severe degradation was expected for this material.

The possible protection offered by scale deposit can be inferred from Fig. 11, which shows views of a Ti-6Al-4V-ELI wearblade (R_C 34) exposed 20.1 h to unacidified 5%-quality inlet with exhaust pH 5.6. The scale deposited during the test had been removed before examination. This wearblade should be compared with that of the same alloy exposed for 20.1 h to acidified brine, Fig. 8. In the SEM views (b and c) of Fig. 11, a number of relatively small and shallow cavities are visible. It appears that, during the initial stages of scale deposition, relatively uniform but shallow erosion occurred along the whole tip surface. Because of rapid scale build-up, this erosion soon became arrested. The fine, cavity-wall structure referred to earlier is clearly seen here along the whole surface, view (d).

Figure 12 shows cross sections of four Co- and Ni-base wearblades exposed 20 h to 5%-quality inlet. The alloys are arranged in order of their relative resistance to degradation. Quite clearly, the two Haynes Co-base alloys underwent considerably less erosion than the Co-Ni-base and Ni-base alloys, even though one of the Co-base alloys, Stellite 6B, has the lowest hardness of the four. Although the two Co-base alloys differ significantly in hardness (R_C 51 vs R_C 37) they differ only slightly in damage. Both MP35N (R_C 46) and Hastelloy C-276 (R_C 43), views (c) and (d), contain significant amounts of Mo: 10 and 16%, respectively. Stellite 6B contains 1.5% Mo, and Haynes 25 contains none. The Cr contents are not too different for the four alloys. For example,

both Haynes 25 and MP35N contain about 20% Cr. Normally, one would expect that Mo would reduce any corrosive contribution to the erosion of these alloys in the acidic reducing brines. However, a key factor of erosion in a corrosive environment is repassivation kinetics, and Mo might have an adverse effect on such kinetics. Alternatively, the high Co content of the two Haynes alloys in contrast to high Ni in the C-276 alloy might be a contributing factor; but contradicting this suggestion is that MP35N has equal and significant amounts of both Ni and Co (35% of each element), yet it suffered severe attack.

Details of damage in terms of surface recession and maximum pit depths observed for all the exposed wearblades are given in a separate report.⁽⁶⁾ Twenty-five wearblades were analyzed. Because of the variable exposure conditions, ranking of the alloys is to be taken with caution. Our attempt of such ranking is shown in the wearblade column of Table II. Although there is some trend between ranking and hardness, there are too many exceptions to consider hardness as being important for erosion resistance in these brines. A similar conclusion on the role of hardness can be drawn from the ranking of the SCC specimens, also shown in Table II.

SCC Specimens

The following figures contain photomicrographs taken of longitudinal-thickness surfaces of SCC specimens. Notations "F" and "R" refer to front- and rear-mounted specimens (Fig. 2(c)). Only tensile-stressed surfaces are shown in the figures, but both tensile

and compressive surfaces were examined. We examined specimens for evidence of SCC, erosion cavities, and corrosion. Eighty-seven specimens were exposed, 80 in pairs (with front and rear specimens) and 7 individually (front only). The predominant mode of degradation observed for most specimens was the formation of cavities due to erosion or corrosion-assisted erosion. Many specimens also showed evidence of SCC. The Ti-base alloys generally showed the greatest resistance to erosion attack. In a separate report ⁽⁶⁾ we characterize the degree of such attack for all specimens in terms of maximum depth of cavities. We also report the presence of stress corrosion cracks in and outside of the notch for each specimen. In the present paper, we present various types of damage observed in SCC specimens.

We included one pair of Ti-8Al-1Mo-1V specimens in each of the first two test series because this material is known to exhibit SCC in aqueous chlorides. ^(4,7) Numerous cracks, up to about 50 μm deep, had developed along the entire tensile surface of these four specimens and at the root of the notch in the two front specimens. Of the remaining Ti-base alloys, only three specimens showed any evidence of surface cracking (outside the notch). These were a Ti-6Al-4V front specimen and two Ti-6Al-4V-ELI front specimens. Surprisingly, the Ti-6Al-4V and one of the Ti-6Al-4V-ELI specimens were exposed to unacidified brine, which should be the least severe of the environments. Figure 13 contains micrographs of several Ti-base alloys, illustrating both SCC and erosion. View (a) shows stress corrosion cracks along the tensile surface of a Ti-8Al-1Mo-1V

specimen. An example of SCC at the notch is shown in view (b) and at a higher magnification in view (c) for a Ti-6Al-4V specimen. Note the crack- and erosion-free surface away from the notch. Cracking appears to be predominantly intergranular. The remaining three views, (d), (e), and (f), are examples of various degrees of erosion typically seen in the Ti-base specimens.

Table III lists the number of specimens of each alloy tested; the two final columns indicate the number that showed cracks in the notch and surface regions respectively. The alloys are not ranked in any order.

Although Ti-6Al-4V-ELI exhibited less susceptibility to SCC than Ti-6Al-4V, it exhibited more susceptibility to erosion. Our ranking of the SCC specimens in terms of erosion is shown in Table II. The limited number of specimens that we tested for most of the alloys and the variable exposure conditions may limit the reliability of such ranking.

The alloy Ti-4Al-3Mo-1V was expected to be one of the most resistant to SCC in chlorides.⁽⁴⁾ Two sets of this alloy were exposed, and cracks were observed in the notch of the two rear specimens. Of the remaining Ti-base alloys, one set of each was exposed, all to about the same environment, in the second test series. The Ti-6Al-6Nb-2Sn was heat treated to a relatively high strength level (DPH 463). It showed no evidence of SCC or erosion; the latter is consistent with the wearblade results for this alloy. The Ti-6Al-2Nb-1Ta-1Mo, which is a high- α alloy, did not exhibit any SCC and showed good resistance to erosion. The remaining five

Ti-base alloys are β -stabilized alloys, which were tested in their low to intermediate strength levels. These alloys were comparable to the Ti-6Al-4V/Ti-6Al-4V-ELI group for their resistance to SCC and erosion when exposed for equal times. For the β alloys, we observed no correlation between degradation and hardness. In all Ti-base alloys the compressive surfaces were not attacked.

Four Ni- and Co-base alloys were tested. Two specimens from this group exhibited considerable degradation, with cavities over 50 μm deep.* View (a) of Fig. 14 shows the extensive erosion encountered in a front specimen of MP35N exposed to acidified 0%-quality inlet for 37 h. Evidence of SCC is also seen, although the cracks were blunted by the excessive erosion. The rear specimen, view (b), showed no degradation. The same alloy exposed 20 h to acidified 5%-quality inlet showed no evidence of SCC and only minor erosion, with cavities in the range of 4 to 10 μm deep. Views (c) and (d) show an extreme example of pitting and SCC in an Inconel 718 front specimen; cracking is predominantly intergranular. The corresponding rear specimen, view (e), was not attacked. The specimens were exposed 60.5 h to acidified 11%-quality inlet. In Inconel 718 specimens that

* Maximum cavity depths were classified according to the scheme:

<3 μm , 4-10 μm , 11-20 μm , 21-50 μm , and >50 μm .

were exposed 18.5 h to acidified 5%-quality inlet, cracks developed only in the notched region and the front specimen was only moderately eroded, with 11- to 20- μm maximum cavity depth. The MP35N and Inconel 718 specimens were in the cold-worked-and-aged conditions.

Three pairs of Hastelloy C-276 specimen were exposed, two pairs in the cold-worked-and-aged (hardened) condition (DPH 407) and the third pair in the annealed condition (DPH 224). One pair of the hardened condition was exposed for 60.5 h to acidified 11%-quality inlet, the other for 20.1 h to acidified 5%-quality inlet. Both pairs showed evidence of SCC, but only in the notched area; both front specimens showed mild erosion attack, with 4- to 10- μm maximum depths. In spite of the large difference in exposure conditions, the extent of degradation in the two pairs was similar. The unhardened pair, which was exposed with one of the hardened pairs for the 20.1-h run, did not show any surface degradation or SCC.

We tested one pair of Haynes 25 specimens. These were not notched and were in the annealed condition. They were exposed for 20.1 h to acidified 5%-quality inlet. Only mild surface degradation was observed, with 4- to 10- μm maximum depths.

Several ferritic stainless steels, ranging from 18Cr-2Mo to 29Cr-4Mo-2Ni, were exposed either 37 or 60 h in the first test series. Out of ten specimens, two developed cracks in the notched region. Erosion in all was mild, with maximum depths less than

10 μm . With the exception of one specimen, none of the compressive surfaces showed any damage. Two high-Ni, austenitic steels (A286, cold rolled and aged (DPH 429), and AL-6X, not heat-treatable (DPH 190)) were exposed 20 h to acidified 5%-quality inlet. Neither showed evidence of SCC; surprisingly, the harder alloy suffered deeper erosion cavities than did the softer alloy, 11 to 20 μm vs less than 4 μm , respectively.

Severe surface erosion/corrosion was observed in a pair of 316 stainless-steel specimens, as shown in Figs. 15(a) and (b). Both front and rear specimens had cavities more than 50 μm deep. Cavities in the front specimen were typical of erosion cavities seen in other alloys. Blunted cracks were frequently present. In contrast, the degradation of the rear specimen occurred by intrusions of pits typical of corrosion attack. Traces of the original surface can still be seen, which is surprising in view of the relatively intense corrosion. The compressive side of both specimens showed no attack. Evidence of sensitization was not detected. A pair of 304 stainless-steel specimens were exposed to conditions similar to those for the 316 stainless-steel specimens: 37 h to acidified 0%-quality inlet, with pH 3.1. These showed only mild surface erosion (4- to 10- μm maximum depth) and no evidence of SCC; the front specimen is shown in Fig. 15(c). The superior resistance to degradation of 304 over 316 stainless steel is surprising.

Figure 15(d) shows severe erosion/corrosion in a front-tested 410 martensitic stainless steel. The specimen was exposed for 37 h to acidified 0%-quality inlet. Several layers of scale deposit

formed, indicating the presence of several high-pH excursions. No scale had deposited on the rear specimen, which was pitted much less but still to a depth greater than 50 μm . Evidence of blunted cracks could be seen. Both specimens contained corrosion pits on their compressive surfaces.

Figure 16 shows micrographs from specimen pairs of 2.2Cr-1Mo steel and 4130-Mo-modified steel; both pairs were quenched and tempered. The front specimens showed extensive attack, with maximum pit depth greater than 50 μm . A series of cracks can be seen in the rear-mounted 2.2Cr-1Mo steel specimen, view (b). Similar cracks appear to be blunted in the more severely eroded/corroded front specimen, view (a). One of the few examples where corrosion product can be seen is in the 4130-Mo-modified specimens. View (c) of Fig. 16 shows a wavy layer of corrosion product that separated from the metal on mounting. View (d) shows a very thin adherent corrosion film, which thickens occasionally into a corrosion pit. The 4130 steel was exposed for only 7.5 h, compared to 37.0 h for the 2.2Cr-1Mo steel; both were exposed to acidified 0%-quality inlet. All four specimens contained corrosion pits on the compressive side.

As is evident in Table III, the ferritic stainless steels as a group appear to exhibit the best resistance to SCC. However, in the absence of notches, and excluding Ti-8Al-1Mo-1V, the Ti-base alloys should offer the best combination of resistance to SCC, erosion, and corrosion. The general lack of correlation between erosion and hardness that was observed for the wearblades is even more evident for the SCC specimens.

DISCUSSION

In a recent review paper, Preece⁽⁸⁾ points out the current inability to formulate a relationship that would, irrespective of the class or condition of a material, relate the resistance to erosion of a material to its properties. The difficulty is that erosion is a complex phenomenon involving a number of material properties. With the added complexity of corrosion and the nonuniform brine conditions, it is not surprising that no systematic correlation between erosion and hardness was obtainable. Furthermore, several reverse results were seen. The general superiority in erosion resistance of the Ti-base alloys over the Ni- and Co-base alloys must at least in part result from the relative rate of surface repassivation of the respective alloys in the brines. The lower resistance of the Mo-containing wearblades (MP35N and C-276) compared to that of the Co-base wearblades (Stellite 6B and Haynes 25) might in fact result from lower repassivation kinetics imparted by Mo, or from higher repassivation kinetics imparted by Co over Ni. The hardnesses of these four alloys apparently have little if any effect on the extent of damage. For the Ti-base alloys, the wearblades show some trend between hardness and erosion resistance but the corresponding ranking of the SCC specimens shows many exceptions. Most of the Ti-base SCC specimens were exposed for 20 h in the second test series, and therefore the variation in erosion resistance cannot be attributed to environment alone. We suggest that for the Ti-base alloys resistance to

corrosion, especially as related to repassivation of their surfaces, greatly affects their resistance to erosion. Beck, in pitting experiments using Ti foils in halogen solutions, showed that repassivation starts instantaneously, and can be completed in less than 1 s.⁽⁹⁾

Cavities or craters resulting from erosion by either solid-particle,⁽¹⁰⁻¹²⁾ liquid-droplet,^(8,13) or cavitation-induced^(8,14,15) impacts have frequently been reported. Associated with these cavities, evidence of plastic deformation was reported at least for ductile materials. At high impact angles, a raised lip usually formed by a Brinelling or extrusion process as the cavity or crater formed. At low impact angles, erosion is generally thought of as resulting primarily from ploughing or micromachining, although these two processes can also occur at high angles once the surface becomes roughened.⁽¹¹⁾ Ripple formation, slip bands, work hardening, fatigue cracking, the propagation of cracks, and hills and valleys formed by local extrusions are all indications of the role plastic deformation plays in erosion studies. Nevertheless, in our work we could not find any visual surface evidence of plastic deformation of the wearblades. We suggest that concomitant corrosion likely obliterates any additive effects of repeated impacts that would normally lead to easily observed plastic deformation.

Considerable evidence exists^(8,16) that, for ductile materials, the erosion rate is greatest at some intermediate impact angle of about 0.35 rad. In our case, the leading-edge tip radius provided a

range of angles from 0.17 to 1.57 rad, but the maximum erosion, as evidenced by the receding and flattening of the tip surface, occurred at about 1.57 rad. This apparent anomaly probably results from a reduction of impact velocity and impact mass that is due to the deflection of the supersonic liquid flow away from the wearblade tip. This deflection would produce a pressure discontinuity, resulting in a pair of lateral shock fronts - one on each side of the wearblade - which will interact with and retard the flow on either side of the tip. If the particles and/or liquid droplets that are primarily responsible for the erosion are of the order of 20 μm or less, then they will be easily deflected along with the liquid vapor flow stream.⁽¹⁷⁾ Although particulate and droplet size were not measured in the field studies, these sizes are within the ranges of water-droplet sizes observed in our laboratory nozzle expansion tests and of particulate sizes observed in our scale deposits.⁽¹⁾

The contribution of secondary damage by fragments from the primary impacts to high-impact-angle erosion was pointed out by Tilly.⁽¹²⁾ But such damage should have resulted in uniform erosion, in contrast to the observed formation of deep cavities. In some cases, evidence of machining marks around these cavities could still be seen on our wearblades. Adler and Hooker, in their studies with water drops, state that once an erosion pit is started, enlargement occurs very rapidly.⁽¹³⁾ The question we pose is why the initial cavities grow to such an extent in the wearblades without significant pitting of the surrounding area, especially for the Ti-base alloys and

the two Co-base alloys. Interestingly, erosion pits for these alloys were quite localized in the SCC specimens as well, whereas in alloys such as MP35N, Hastelloy C-276, Inconel 718, and many of the stainless steels such erosion was continuous along the entire tensile surface.

The fine structure of the surfaces of the wearblade cavities is not too different from that shown by Beck in pitting studies on Ti.⁽¹⁸⁾ This suggests that corrosion could be an important factor in the growth of these cavities. We propose that, in the acidified two-phase flow, the damage from particulates and water droplets occurs at a low enough rate that the surfaces of the Ti-base alloys are readily repassivated. This would also account for the relatively little damage seen in these alloys for the short runs (less than 20 h). However, once a critical-size cavity forms, liquid becomes entrapped and continuously becomes more concentrated and more acidic, making repassivation more difficult. As the cavity grows, corrosion continuously becomes more dominant than erosion; the process is autocatalytic, typical of pitting corrosion⁽¹⁹⁾ and the degradation continuously accelerates. For alloys where the repassivation kinetics are relatively slow, critical-size cavities form more readily and are more numerous. This should lead to more of a general surface recession, as was observed for the Hastelloy C-276 wearblade. In the extreme, the whole wearblade tip and tapered surface will corrode away. This occurred with the 2.2Cr-1Mo steel wearblade. That the fine structure of the cavity walls in the Co- and Ni-base alloys had a more open or void-like appearance than in the Ti-base alloys could be explained by the more rapid corrosion of these non-Ti-base alloys.

The analyses of the SCC specimens indicate the synergism between erosion and corrosion. Even in cases where significant erosion/corrosion was observed for the front specimens exposed to the direct impact from the nozzle exhaust, such as Inconel 718 and MP35N, no damage could be detected for the shielded rear specimens. The extensive damage encountered on the tensile surface of the shielded, rear 316 stainless-steel specimen suggests that for this specimen corrosion was a dominant factor. However, no degradation was observed on the compressive surface of either the front or the rear specimen. It appears that not only erosion of the protective oxide film but also tensile stresses aid in inducing and maintaining corrosive actions, and such stresses become especially important where corrosion is prominent. Normally, one would expect that SCC would dominate in the presence of stress, but evidently in many cases corrosion, or erosion combined with corrosion, progresses fast enough to blunt the cracks as they develop. Evidence of crack blunting was clearly seen in a number of specimens, e.g., the front 316 stainless-steel specimen. For the medium- and low-alloy steels, corrosion was evident on both tensile and compressive surfaces but to a much greater extent on the tensile surface; this clearly indicated the role of tensile stresses as well as erosion on accelerating corrosion.

Table II shows that there is a large contradiction in the ranking of the Ni- and Co-base alloys between the SCC specimens and the wearblades. For example, in SCC the Hastelloy C-276 specimens were ranked considerably above the Haynes 25 specimens, but the reverse

ranking was evident for the corresponding wearblades. The two Haynes 25 specimens and two of the six C-276 SCC specimens were exposed for 20 h in the second test series with the four Ni- and Co-base wearblades of Fig. 12. Both pairs of SCC specimens were in the as-annealed condition, with the Haynes 25 being harder than the C-276; the corresponding wearblades were in the hardened conditions. Neither pair of specimens showed evidence of cracks. However, only the front Haynes 25 specimen was eroded, although with relatively shallow cavities: 4- to 10- μm maximum depth. This reversal in ranking between wearblades and SCC specimens indicates that the presence of concomitant stress can greatly modify the propensity to erosion or corrosion-assisted erosion.

The rate of stress corrosion cracking, especially of crack initiation, depends strongly on stress level, microstructure, alloy strength, and environment. Because our tests did not permit a systematic study of these factors, the ranking of the alloys must be considered only tentative. In addition, it is difficult to explain what environmental factors caused the extensive attack on 316 stainless steel and Inconel 718. The scale deposits on one of the 410 stainless-steel specimens is also curious.

Thus, at best we can only make some general comments with reference to SCC. Except for these isolated anomalies, there appears to be no significant distinction in the susceptibility of the various alloys to SCC. Of the more corrosion-resistant alloys, the Ti-base alloys do show the greatest tendency for crack formation in the

presence of a notch. However, many of these Ti-base alloys show promise for use with notch-free surfaces. Furthermore, all but four of the Ti-base SCC specimens were loaded into the plastic range, considerably above normal working stresses. Taking into account both erosion and SCC, we suggest that the Ti-base alloys would best resist degradation from the nozzle exhaust of acidified, highly mineralized two-phase brine at 104°C.

SUMMARY

A number of Ti-, Fe-, and Co-base alloys in the form of nozzles, wearblades, and stress corrosion cracking (SCC) specimens were exposed to high-velocity, high-salinity, highly mineralized brines in chemistry-oriented nozzle-expansion tests. These tests were carried out in the geothermal field. Testing was performed to evaluate the feasibility of scale control by acidification of the brine with HCl. Three series of tests were run, with exposures of specimens ranging from 7.5 to 120.6 h. Both 100%-liquid and mixed liquid/vapor inlets to the nozzle were used. Fluids were expanded to atmospheric pressure at 104°C.

Erosion of wearblades occurred by the formation and growth of cavities concentrated along the center of the wearblade tips. The tip surface recedes in the direction of the flow and becomes flattened, indicating that erosion was most effective at impact angles close to 1.57 rad.

The Ti-base alloys show the best resistance to erosion for both wearblades and SCC specimens. Although erosion resistance generally increased with increasing hardness for the Ti-base alloys, no correlation between erosion resistance and hardness was obtained for other alloys or for all the alloys taken together. The erosion-resistance rankings based on both wearblade and SCC specimens did not agree for the Ni- and Co-base alloys.

Because the fine structure of the cavity walls is similar to that of electrochemically pitted surfaces, we propose that degradation occurs by corrosion-assisted erosion and that it is largely controlled by repassivation kinetics. The formation of critical-size, stable cavities must be inversely related to the ability of the surface to repassivate. Once cavities form, they grow at an accelerating rate by erosion assisted by corrosion pitting. Differences in ranking between wearblades and SCC specimens might be attributed to the different erosion/corrosion environments of the two locations or to differences in the contribution of stress to corrosion-assisted erosion. For alloys with stable passive films, degradation (except where SCC might occur) is not induced by the presence of tensile stress. However, for soluble oxide films, such as with the low- or intermediate-alloy steels, tensile stress will accelerate corrosion or pitting even in the absence of erosive attack. The synergism between erosion, corrosion, and tensile loading is expected to result in the greatest rate of degradation.

Evidence of stress corrosion cracking was seen in each of the alloy groups. Taking into account both erosion and SCC, we suggest that the Ti-base alloys offer the best resistance to degradation in the high-velocity, two-phase, acidified brine at 104^oC.

ACKNOWLEDGMENTS

The authors wish to thank George E. Tardiff for his encouragement and support in this study and Robert E. Garrison for his help with the preparation of specimens. The SEM analyses were provided by Wayne J. Steele. The 4130-steel specimens were provided by R. F. Hehmann, Case Western Reserve University. Heat treatment of test materials was done by Fay A. Dishong. A number of people were involved in the field studies, and the authors wish to acknowledge their support.

REFERENCES

1. A. L. Austin, A. W. Lundberg, L. B. Owen, and G. E. Tardiff, The LLL Geothermal Energy Program Status Report - January 1976-January 1977, Lawrence Livermore Laboratory Report, UCRL-50046-76 (1977).
2. George E. Tardiff, LLL Total Flow Geothermal Program: Summary of Two-Phase Nozzle Tests for Scale Control and Materials Performance, Lawrence Livermore Laboratory Report, UCID-17636 (1977).
3. Fundamental Aspects of Stress Corrosion Cracking, eds. R. W. Staehle, A. J. Forty, and D. van Rooyen, Nat. Assoc. Corr. Eng., Houston, 1969.
4. M. J. Blackburn, J. A. Feeney, and T. R. Beck, "Stress Corrosion Cracking of Titanium Alloys," in Advances In Corrosion Science and Technology, eds., M. G. Fontana and R. W. Staehle, vol. 3, Plenum Press, New York, p. 67, 1973.
5. R. L. Cowan and C. S. Tedman, Jr., "Intergranular Corrosion of Iron-Nickel-Chromium Alloys," *ibid.*, p. 293.
6. Alfred Goldberg and Robert P. Kershaw, Evaluation of Materials Exposed to Expanded Geothermal Brine, Lawrence Livermore Laboratory report, in draft form.
7. T. R. Beck, "Stress Corrosion Cracking of Titanium Alloys," J. Electrochem. Soc. 114, 551 (1967).
8. C. M. Preece, "Erosion," Ann. Rev. Mater. Sci. 7, 95 (1977).

9. T. R. Beck, "Pitting of Titanium," J. Electrochem. Soc. 120, 1310 (1973).
10. I. M. Hutchings and R. E. Winter, "Particle Erosion of Ductile Metals: A Mechanism of Material Removal," Wear 27, 121 (1974).
11. J. W. Edington and I. G. Wright, "Study of Particle Erosion Damage in Haynes Stellite 6B: Scanning Electron Microscopy of Eroded Surfaces," Wear 48, 131 (1978).
12. G. P. Tilly, "A Two-Stage Mechanism of Ductile Erosion," Wear 23, 87 (1973).
13. W. F. Adler and S. V. Hooker, "Water Drop Impact in Zinc Sulfide," Wear 48, 103 (1978).
14. B. Vyas and C. M. Preece, "Cavitation-Induced Deformation of Aluminum," in Erosion, Wear, and Interfaces with Corrosion, Special Technical Publication 567, ASTM, Philadelphia, p. 77, (1974).
15. F. Erdmann-Jesnitzer and H. Louis, "Studies on Cavitation Damage," *ibid.*, p. 171.
16. I. Finnie, "Some Observations on the Erosion of Ductile Metals," Wear 19, 81 (1972).
17. G. P. Tilly and W. Sage, "The Interaction of Particle and Material Behavior in Erosion Processes," Wear 16, 447 (1970).
18. T. R. Beck, "Pitting of Titanium," J. Electrochem Soc. 12, 1317 (1973).
19. A Goldberg and L. B. Owen, "Pitting Corrosion and Scaling of Carbon Steels in Geothermal Brine," to be published in Corrosion.

NOTICE

"This report was prepared as an account of work sponsored by the United States Government. Neither the United States nor the United States Department of Energy, nor any of their employees, nor any of their contractors, subcontractors, or their employees, makes any warranty, express or implied, or assumes any legal liability or responsibility for the accuracy, completeness or usefulness of any information, apparatus, product or process disclosed, or represents that its use would not infringe privately-owned rights."

Table I. Changes in brine conditions and composition during tests (from Ref. 1).^a

	Date			
	6/29/76	6/30/76	8/8/76	8/10/76
Temperature, °C	200	214	230	215
Pressure, MPa (gage)	1.55	1.65	2.21	1.62
pH		5.7	5.8	6.1
Oxidation-reduction potential, mV vs H ₂			192	177
Density, g/cm ³	1.12	1.12	1.13	1.14
Total solids, g/kg brine by evaporation	169	171	197	196
Elemental composition, ppm (wt.)				
Lithium			128	135
Sodium	40 900	42 100	41 200	42 700
Silicon	181	187	190	200
Potassium	6 900	7 000	6 600	6 500
Iron	202	161	199	180
Copper	1	1	1	1
Barium	54	85	115	118
Magnesium	125	125	95	99
Zinc	188	183	275	285
Strontium			360	373
Tin	23	23		
Aluminum				<1
Chlorine	101 000	105 000	111 000	112 000
Calcium	17 400	16 900	17 900	18 200
Manganese	502	494	565	570
Antimony	4	4		
Lead	22	22	60	59

^aSteam quality 10%. Concentrations have not been corrected for flashing; brine samples were obtained from the LLL separator.

Table II. Ranking on basis of surface recession and cavities. Alloys are listed in order of increasing degradation.

Wearblades			SCC specimens ^a		
No. specimens	Alloy	Hardness, R _C	No. specimens	Alloy	Hardness, R _C
1	Ti-6Al-6V-2Sn	43	1	Ti-6Al-6Nb-2Sn	463
3	Ti-6Al-4V	34-37	1	Ti-3Al-8Mo-8V-2Fe	416
2	Ti-6Al-4V case hardened in CH ₄ /N ₂ /H ₂	37 (750) ^b	1	Ti-3Al-15V-3Cr-3Sn	363
7	Ti-6Al-4V-ELI	30-34	1	Ti-3Al-10V-2Fe	355
1	Haynes 25: Co-20Cr-14.5W-9.5Ni-2.5Fe	51	8	Ti-6Al-4V	324-342
1	Stellite 6B: Co-30Cr-4.5W-2.5Ni-1Mo-1C	37	1	Ti-6Al-2Nb-1Ta-1Mo	361
1	Haynes 25	20	3	Hastelloy C-276	224-407
1	Ti-6Al-2Nb-1Ta-1Mo	32	1	AL-6X: Fe-20Cr-24Ni-6.5Mo	190
2	MP35N: 35Co-35Ni-20Cr-9.5Mo	46-47	1	Fe-29Cr-4Mo-2Ni	251
3	Hastelloy C-276: Ni-16Cr-15.5Mo-5.5Fe-3.3W	10-47	7	Ti-6Al-4V-ELI	336-354
1	Ti-0.3Mo-0.8Ni	6	1	Ti-3Al-8V-6Cr-4Mo-4Zr	418
1	Ti-6Al-4V - plasma spayed with 90Ta-10W	45	1	Ti-11.5Mo-6Zr-4.5Sn	350
1	2.2Cr-1Mo Steel	21	2	Fe-29Cr-4Mo	238
			2	Ti-8Al-1Mo-1V	345
			2	Ti-4Al-3Mo-IV	284
			1	Fe-18Cr-2Mo	203
			1	Haynes 25	285
			1	304 Stainless Steel	192
			2	MP35N	514
			1	A-286: Fe-26Ni-14.5Cr-1.2Mo-2Ti-0.35Al	429
			2	Inconel 718: Ni-19Cr-18Fe-5(Nb+Ta)-3Mo-0.9Ti-0.5Al	520
			1	316 Stainless Steel	185
			1	2.2Cr-1Mo Steel	260
			2	4130 Steel	254-262
			1	410 Stainless Steel	243

^aOnly front SCC specimens are listed.

^bDPH (microhardness) maximum of hardened case.

Table III. Evidence of SCC in bent-beam specimens.
(Specimens are not listed in any ranking order.)

No. specimens tested	Alloy	Hardness, DPH	No. specimens showing cracks	
			In notch	On surface
11	Ti-6Al-4V-ELI	324-342	0	2
13	Ti-6Al-4V	336-354	9	3
4	Ti-4Al-3Mo-1V	284	2	0
4	Ti-8Al-1Mo-1V	345	2	4
2	Ti-6Al-2Nb-1Ta-1Mo	361	0	0
2	Ti-6Al-6Nb-2Sn	463	0	0
2	Ti-3Al-8V-6Cr-4Mo-4Zr	418	1	0
2	Ti-3Al-8Mo-8V-2Fe	416	0	0
2	Ti-3Al-10V-2Fe	355	0	0
2	Ti-3Al-15V-3Cr-3Sn	363	2	0
2	Ti-11.5Mo-6Zr-4.5Sn	350	1	0
4	Hastelloy C-276	407	3	0
2	Hastelloy C-276	224	- ^a	0
2	Inconel 718	520	-	1
2	Inconel 718	520	2	0
4	MP35N	514	0	1
2	Haynes 25	285	-	0
2	AL-6X	190	0	0
2	Fe-29Cr-4Mo-2Ni	251	-	0
4	Fe-29Cr-4Mo	238	2	0
2	Fe-26Cr-1Mo-0.3Ti	188	0	0
2	Fe-18Cr-2Mo	203	0	0
2	A286 SS	429	-	0
2	316 SS	185	0 (P) ^b	1 (P)
2	304 SS	192	0	0
1	410 SS	243	-	(P)
1	410 SS	243	(P)	1
1	2.2Cr-1Mo steel	260	-	1
1	2.2Cr-1Mo steel	260	(P)	(P)
3	4130 steel	251	-	(P)

^aIndicates absence of notch.

^bThe letter P indicates excessive pitting.

FIGURE CAPTIONS

- Fig. 1. Test assembly for scale and materials evaluation in nozzle-expansion field tests.
- Fig. 2. Exposed test assembly and exposed wearblades with stress corrosion cracking specimens. View (b) shows a combination of erosion and corrosion of 2.2Cr-1Mo steel. View (c) shows the nozzle exhaust flow pattern on erosion/corrosion-resistant Ti-6Al-4V.
- Fig. 3. Cross sections of Stellite 6B nozzle insert (R_C 38) exposed 60.5 h to 11%-quality inlet, exhaust pH 2.4: A, erosion gouges; B, scale deposit; C, scale flaked off.
- Fig. 4. Cross sections of Ti-6Al-4V monolithic nozzle (R_C 39) exposed 60.5 h to 11%-quality inlet, exhaust pH 2.3: A, elliptical ridge of heavy scale deposit; B, scale-free surface; C, superficial scale deposits.
- Fig. 5. Surface traces along the tip of the leading edge of (a) Ti-6Al-4V (R_C 36) and (b) Hastelloy C-276 (R_C 46) wearblades exposed to 11%-quality inlet for 60.5 and 49.5 h at exhaust pH 2.4 and 2.3, respectively. The letter A denotes region outside of direct nozzle exhaust with no erosion. Note difference in vertical scales between (a) and (b).
- Fig. 6. Ti-6Al-4V wearblade (R_C 36) exposed to 11%-quality inlet for 60.5 h at exhaust pH 2.4. Views (b) and (c) are higher magnifications of tapered surface and tip shown in view (a).

Fig. 7. Hastelloy C-276 wearblade (R_C 46) exposed to 11%-quality inlet for 49.5 h at exhaust pH 2.3. Views (b) and (c) are higher magnifications of tapered surface and tip shown in view (a).

Fig. 8. Ti-6Al-4V-ELI wearblades exposed to 5%-quality inlet with exhaust pH 3.4: (a), (c), (e), and (g) for 20.1 h (R_C 32) and (b), (d), (f), and (h) for 120.6 h (R_C 34). Arrows in (c) and (d) indicate the flattened tip region.

Fig. 9. Hastelloy C-276 wearblades: (a), (c), and (e)—mill-annealed condition (R_C 10) exposed 37 h to 0%-quality inlet, exhaust pH 2.9; (b), (d), and (f)—60% cold rolled and aged 100 h at 500°C (R_C 43), exposed 20.1 h to 5%-quality inlet, exhaust pH 3.4.

Fig. 10. Cross section of a leading edge showing severe erosion/corrosion of a quenched-and-tempered 2.2Cr-1Mo steel (R_C 21) wearblade exposed 37 h to 0%-quality inlet, exhaust pH 2.6.

Fig. 11. Ti-6Al-4V-ELI wearblade (R_C 34) exposed 20.1 h to unacidified 5%-quality inlet, exhaust pH 5.6.

Fig. 12. Cross sections of four wearblades exposed about 20 h to 5%-quality inlet: (a) Haynes 25 (33% cold rolled + 100 h at 500°C , R_C 51) 20.1 h, exhaust pH 3.7; (b) Stellite 6B (mill annealed + 11% cold rolled, R_C 37) 18.5 h, exhaust pH 3.7; (c) MP35N (50% cold rolled + 4 h at 538°C , R_C 46) 20.0 h, exhaust pH 3.6; (d) Hastelloy C-276 (60% cold rolled + 100 h at 500°C , R_C 43) 20.1 h, exhaust pH 3.4.

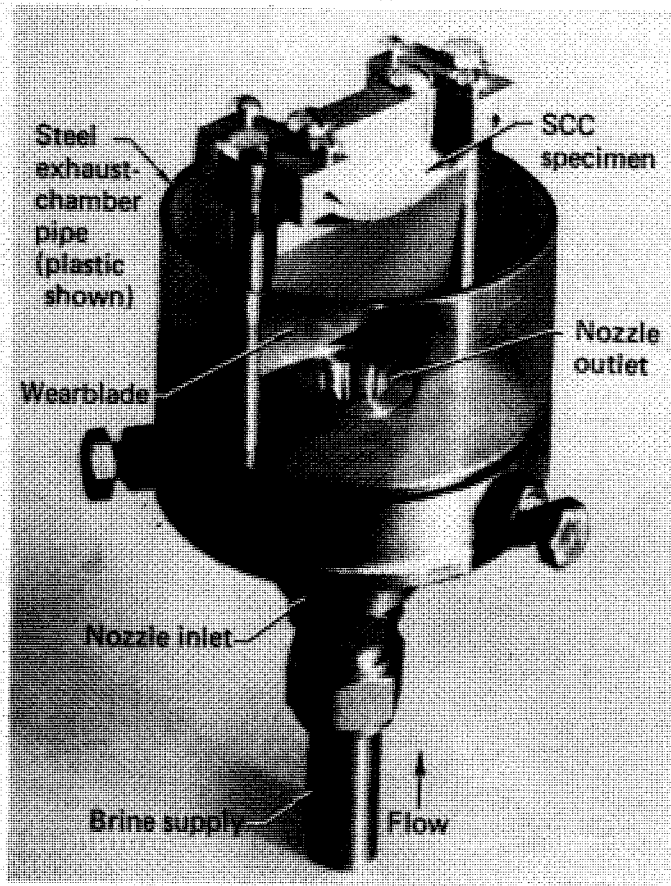
Fig. 13. Examples of exposed Ti-base SCC specimens:

(a)—Ti-8Al-1Mo-1V (DPH 345) 25 h to 0%-quality inlet, exhaust pH 3.9; (b), (c), and (d)—Ti-6Al-4V (DPH 334) 110.5 h to 0%-quality inlet, exhaust pH 3.0; (e)—Ti-6Al-4V (DPH 342) 60.5 h to 11%-quality inlet, exhaust pH 2.4; (f)—Ti-6Al-4V-ELI (DPH 336) 60.5 h to 11%-quality inlet, exhaust pH 2.4. The letters F and R refer to front and rear specimens.

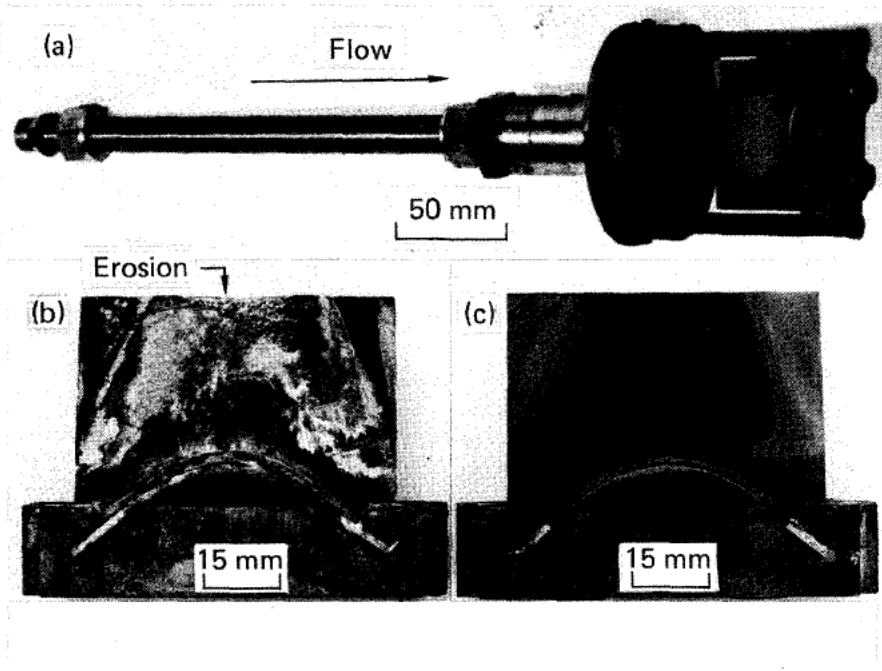
Fig. 14. Examples of exposed Ni- and Co-base SCC specimens: (a) and (b)—MP35N (DPH 514) 37 h to 0%-quality inlet, exhaust pH 3.1; (c), (d), and (e)—Inconel 718 (DPH 530) 60.5 h to 11%-quality inlet, exhaust pH 2.3.

Fig. 15. Examples of exposed stainless steel (SS) SCC specimens: (a) and (b)—316 SS (DPH 185), (c)—304 SS (DPH 192), all three exposed 37 h to 0%-quality inlet, exhaust pH 3.1; (d) and (e)—410 SS (DPH 243) 37 h to 0%-quality inlet, exhaust pH 2.6.

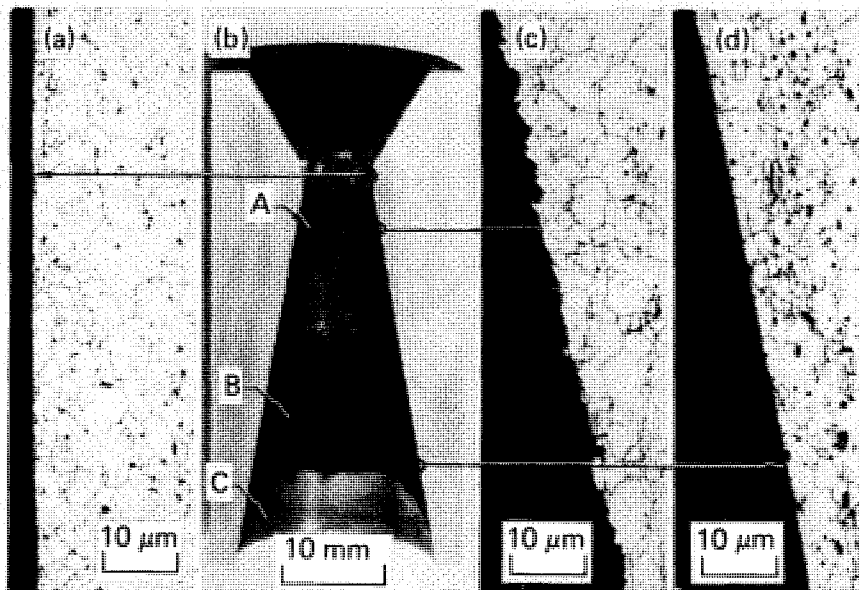
Fig. 16. Examples of exposed quenched-and-tempered medium alloy steel SCC specimens: (a) and (b)—2.2Cr-1Mo (DPH 260) 37 h to 0%-quality inlet, exhaust pH 2.6; (c) and (d)—4130-Mo-modified (DPH 262) 7.5 h to 0%-quality inlet, exhaust pH 2.7. Arrows in (c) and (d) point to corrosion product.



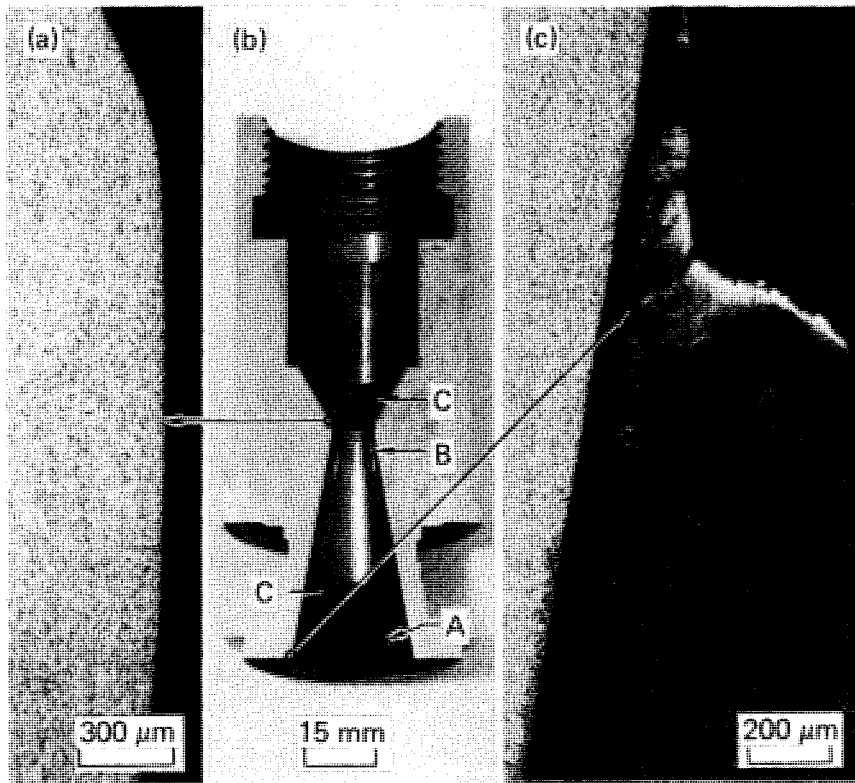
Goldberg - Fig. 1



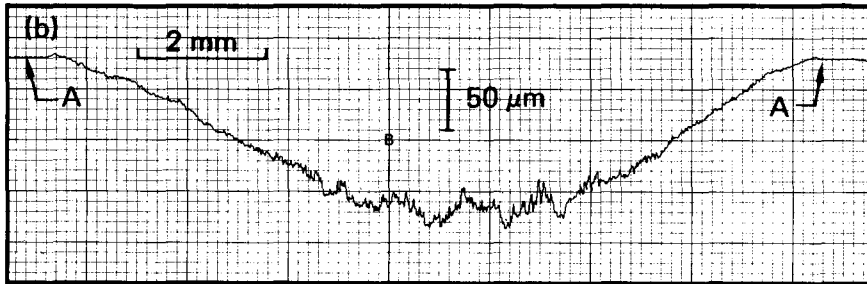
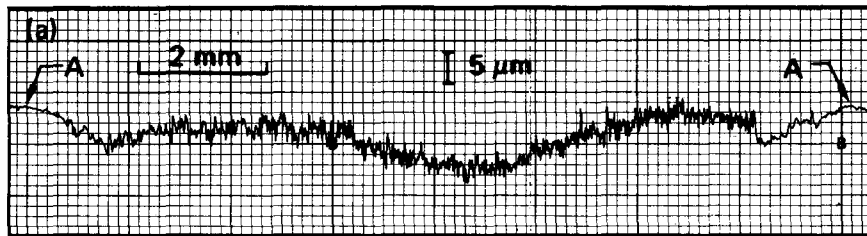
Goldberg - Fig. 2



Goldberg - Fig. 3

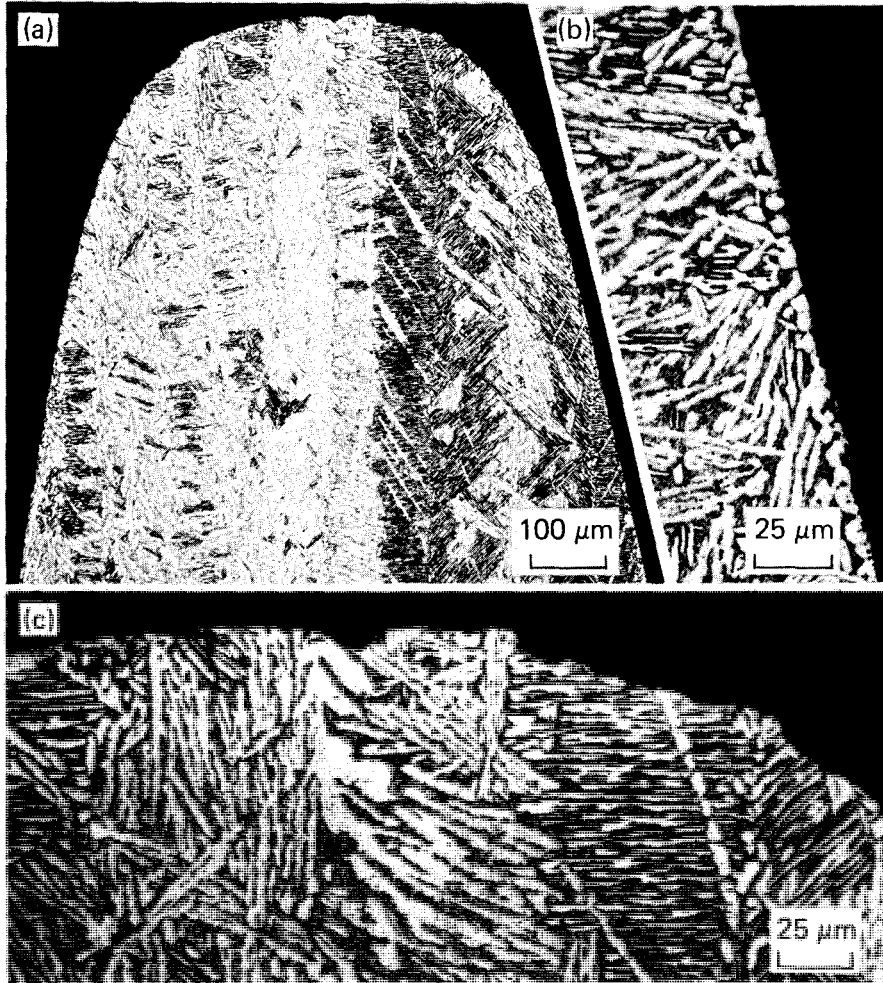


Goldberg - Fig. 4



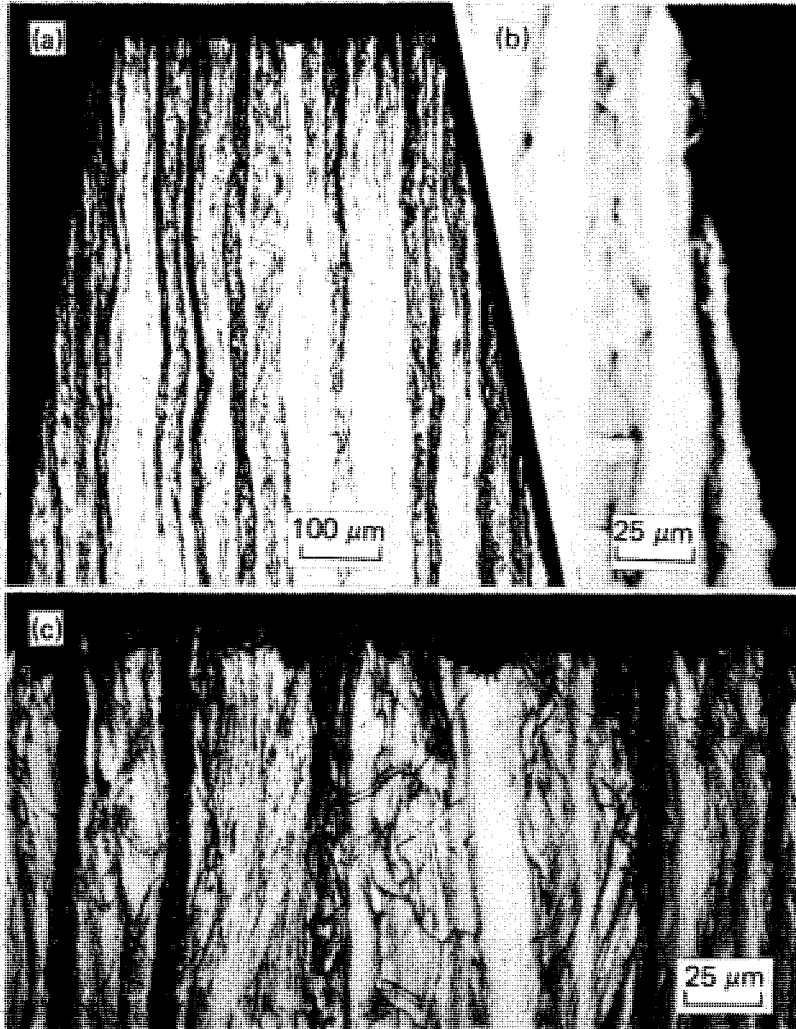
Goldberg - Fig. 5

Ti-6Al-4V

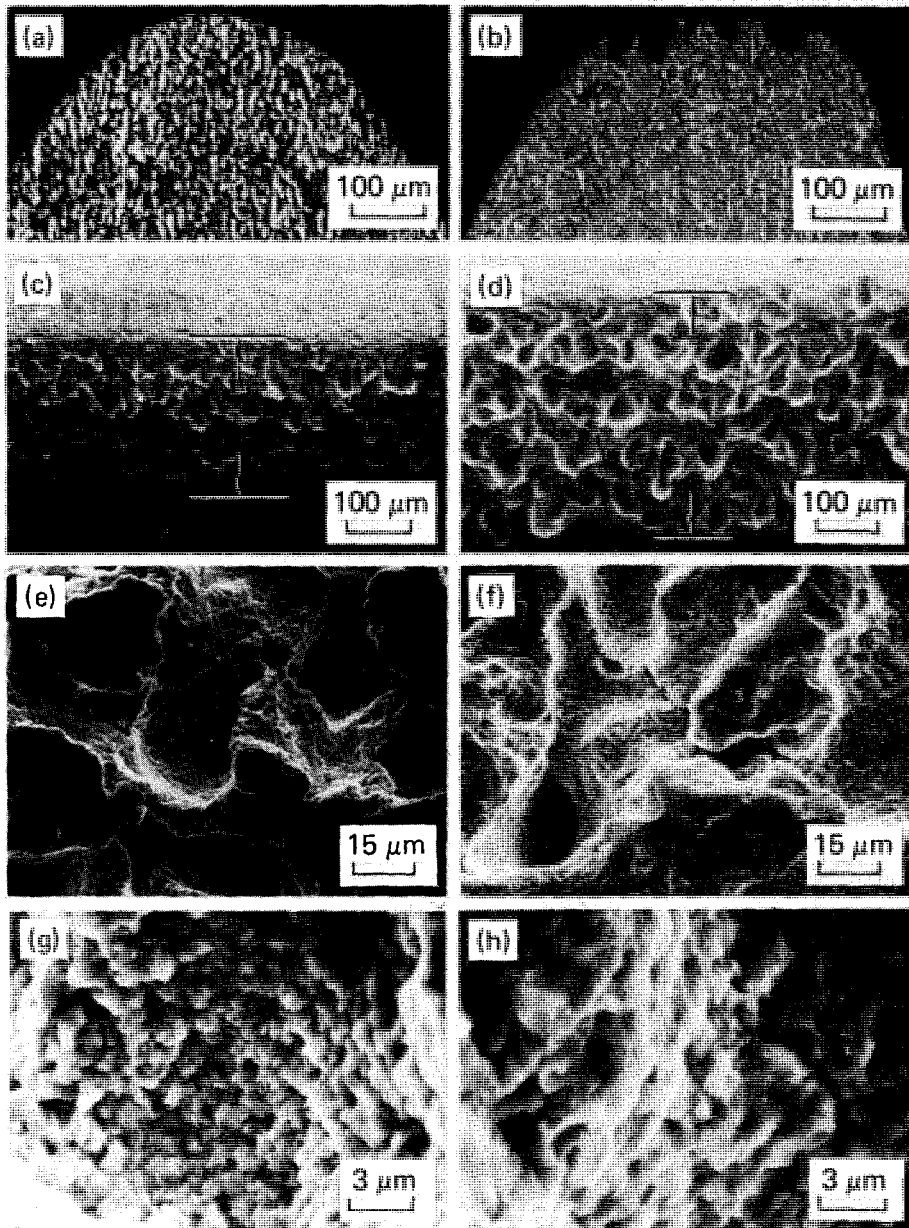


Goldberg - Fig. 6

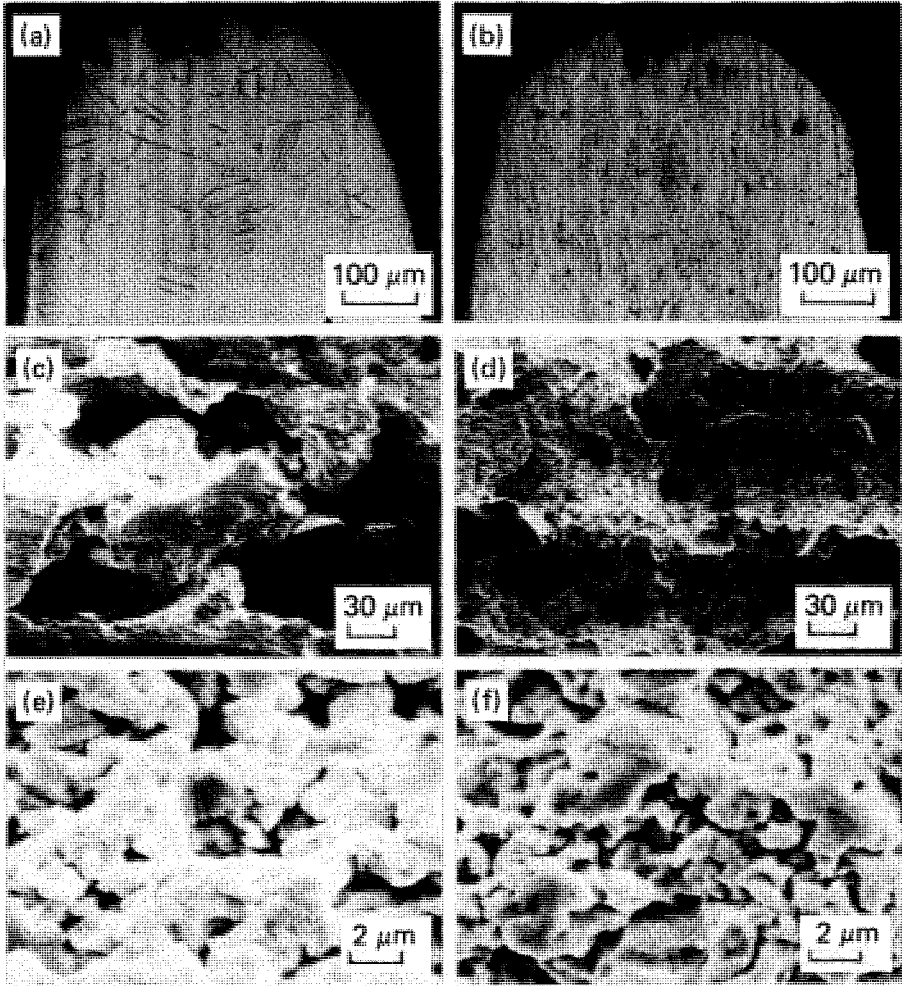
Hastelloy C-276



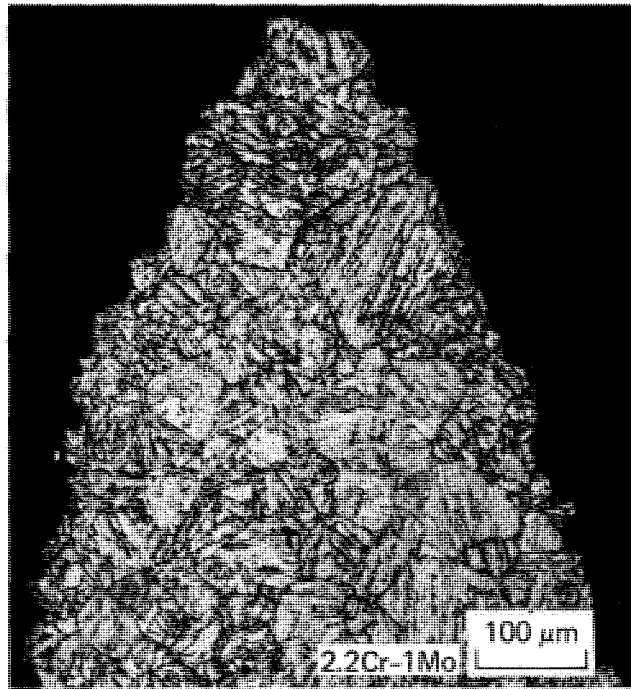
Goldberg - Fig. 7



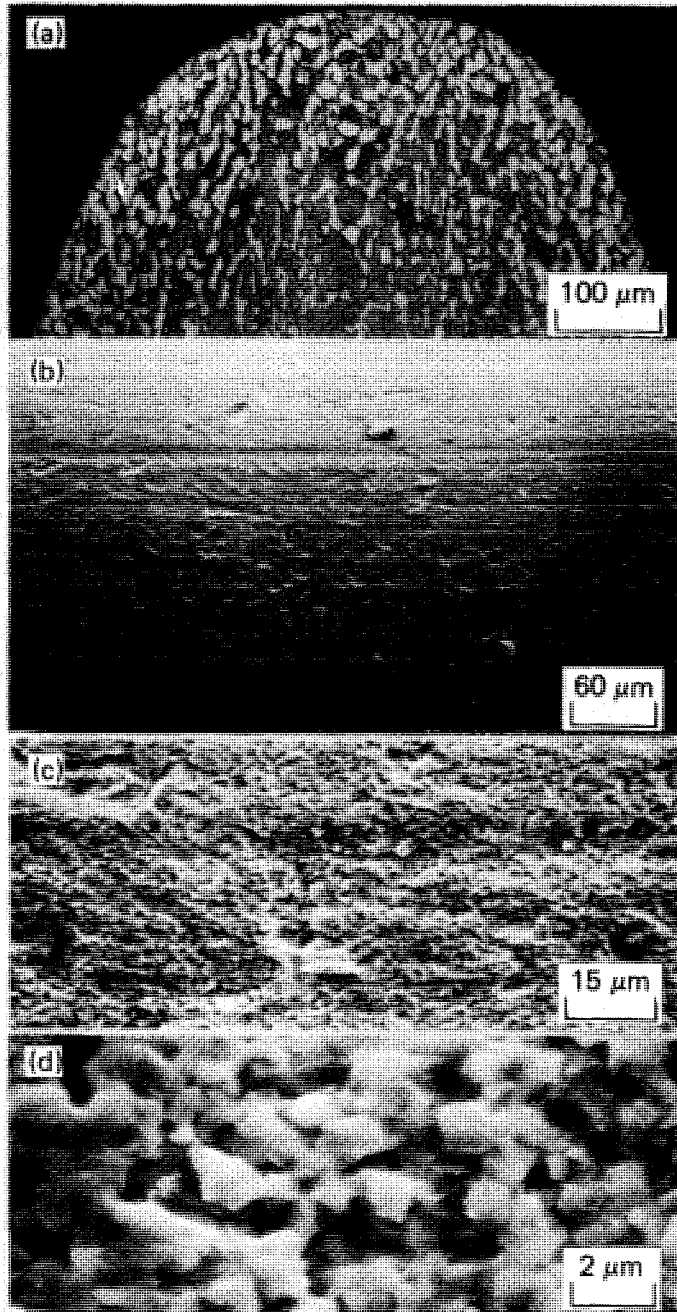
Goldberg - Fig. 8



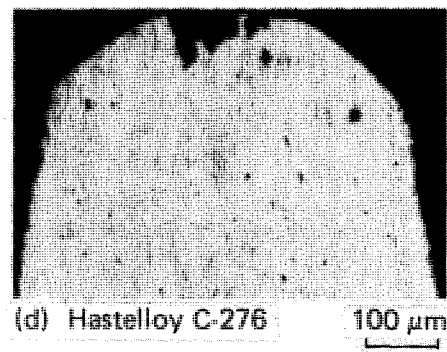
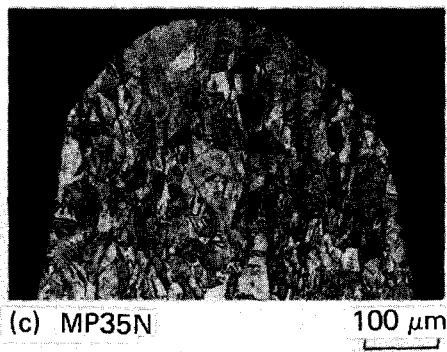
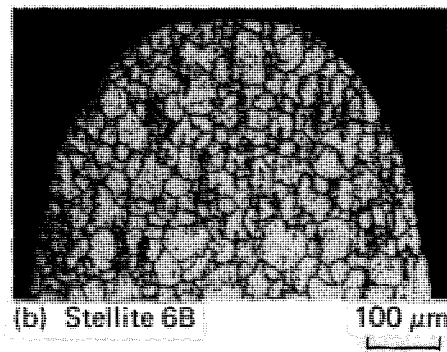
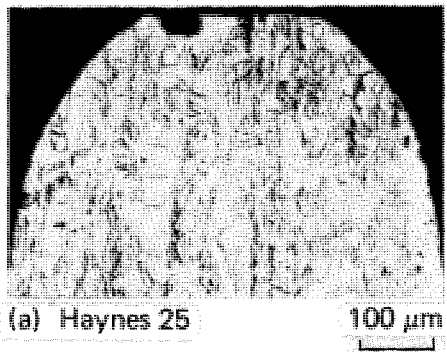
Goldberg - Fig. 9



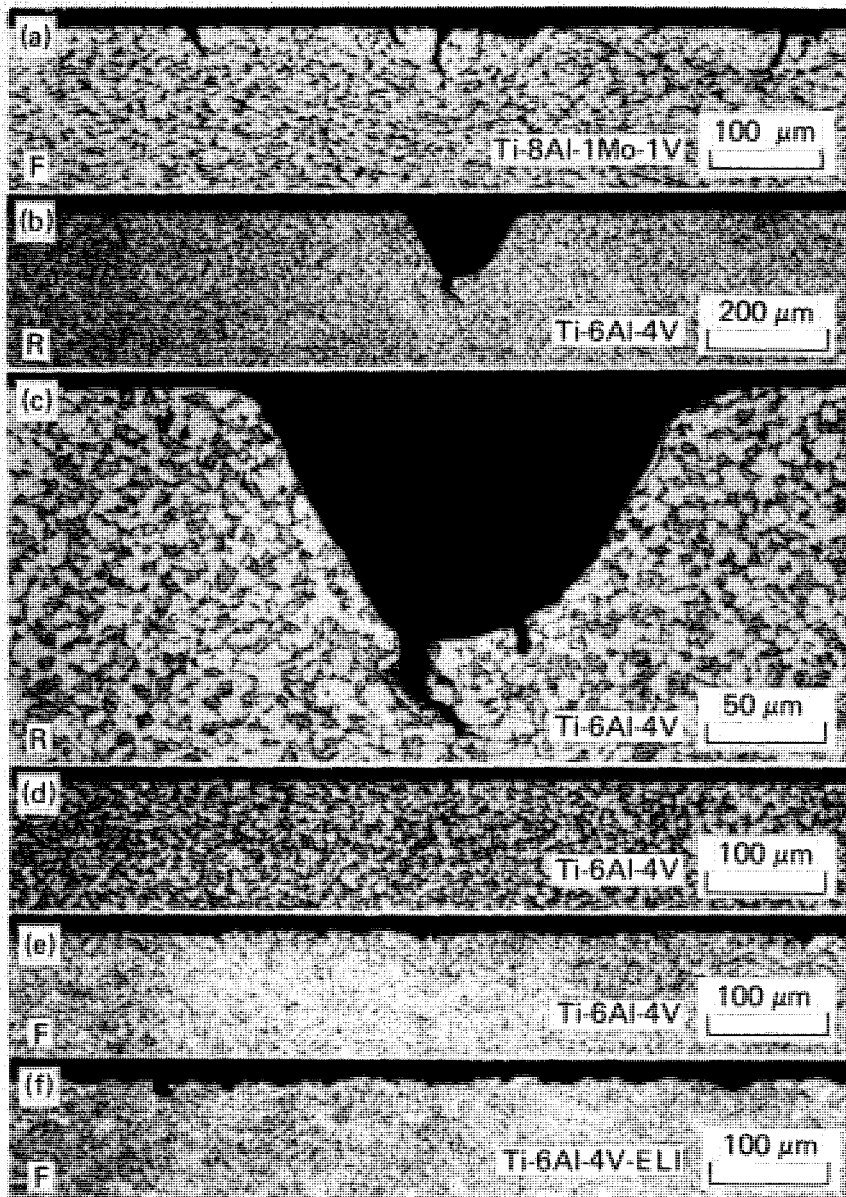
Goldberg - Fig. 10



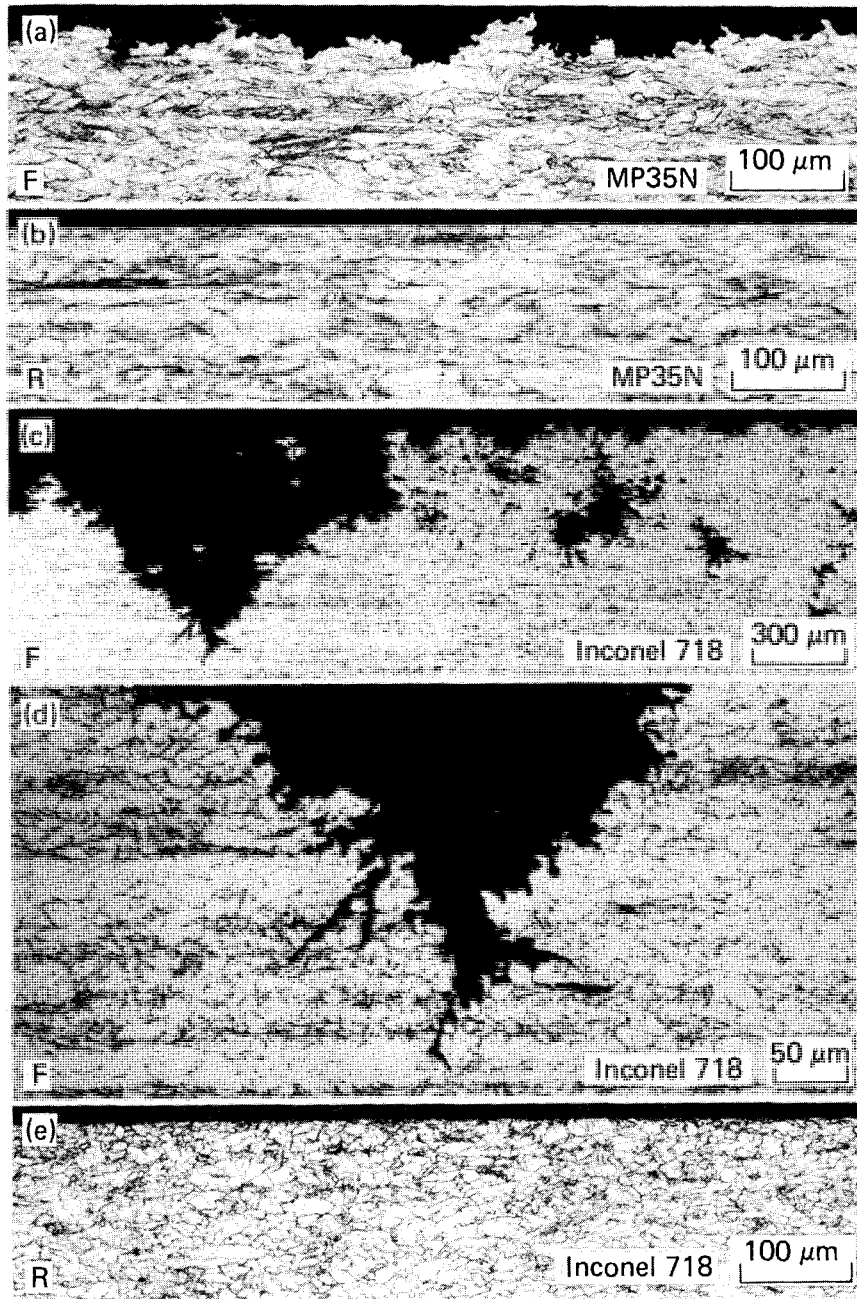
Goldberg - Fig. 11



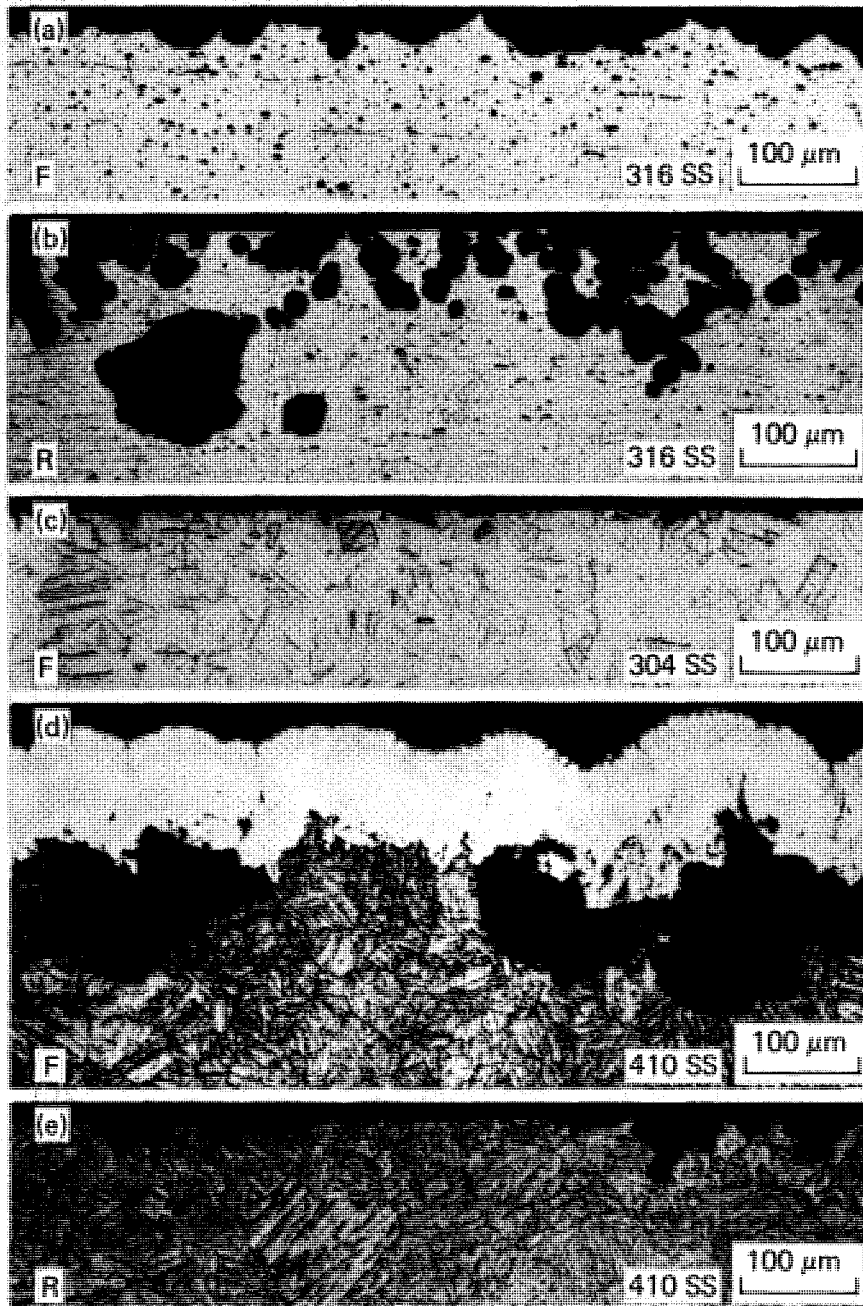
Goldberg - Fig: 12



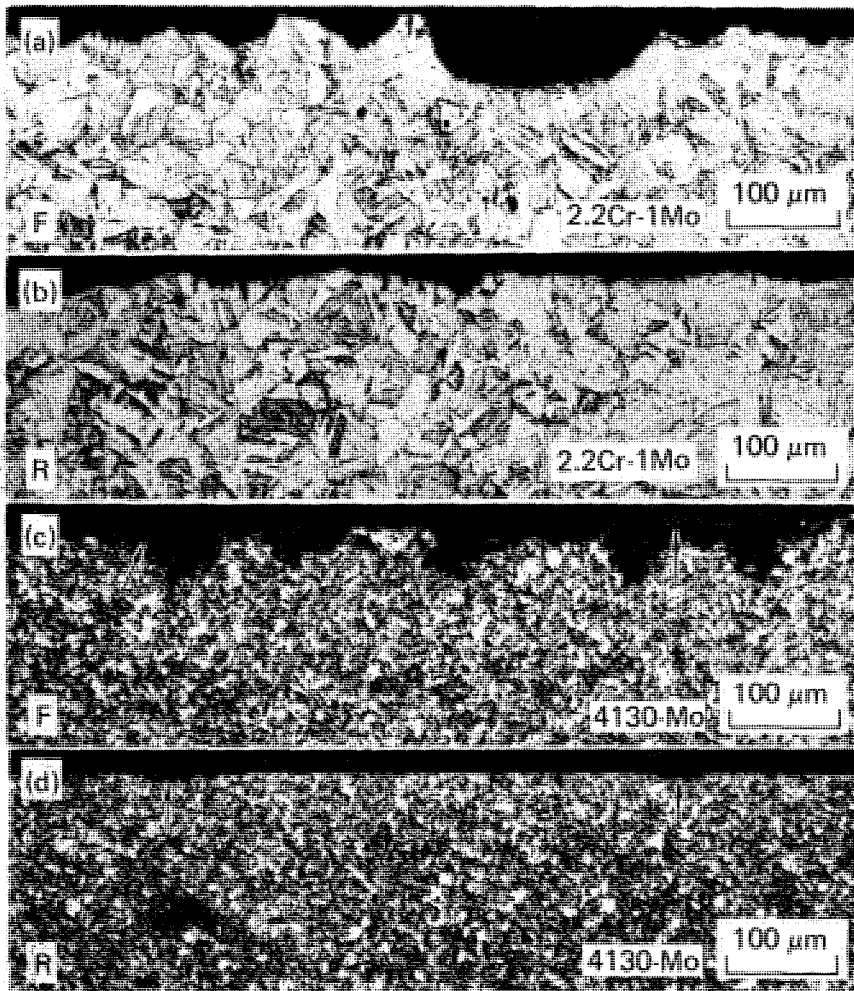
Goldberg - Fig. 13



Goldberg - Fig. 14



Goldberg - Fig. 15



Goldberg - Fig. 16

Technical Information Department
LAWRENCE LIVERMORE LABORATORY
University of California | Livermore, California | 94550

179 683

VAULT REFERENCE COPY

RECEIVED
LAWRENCE LIVERMORE LABORATORY

OCT 02, 1978

TECHNICAL INFORMATION DEPARTMENT